A layerwise geometric error compensation procedure for Additive Manufacturing

Abstract

Purpose: This work provides a new procedure for in-plane compensation of geometric errors that often appear in the layers deposited by an additive manufacturing process when building a part, regardless of the complexity of the layer geometry.

Design/methodology/approach: The procedure is based on comparing the real layer contours to the nominal ones extracted from the STL model of the part. Considering alignment and form deviations, the compensation algorithm generates new compensated contours that match the nominal ones as closely as possible. To assess the compensation effectiveness, two case studies were analysed. In the first case, the parts were not manufactured but the distortions were simulated using a predictive model. In the second example, the test part was actually manufactured and the distortions were measured on a CMM.

Findings: The geometric deviations detected in both case studies, as evaluated by various quality indicators, reduced significantly after applying the compensation procedure, meaning that the compensated and nominal contours were better matched both in shape and size.

Research limitations/implications: Although large contours showed deviations close to zero, dimensional overcompensation was observed when applied to small contours. The compensation procedure could be enhanced if the applied compensation factor took into account the contour size of the analysed layer as well as other geometric parameters that could have an influence.

Originality/value: The presented method of compensation is applicable to layers of any shape obtained in any AM process.

Keywords: Additive Manufacturing, Layerwise, Geometric deviations, Error compensation.

1. Introduction

Despite the competitive advantages of additive manufacturing (AM) (e.g., reduction of overall production time and cost), this technology has not reached yet a sufficient level of maturity for industrial application compared to other conventional manufacturing methods (Gibson et al., 2010). The scarcity of standards regulating the implementation of AM, together with the limitations of tools and methodologies for quality assurance (e.g., structural, dimensional, and geometric) in these manufacturing techniques, has prompted numerous research efforts to improve the capabilities of this technology (Tofail et al., 2018).

Factors such as CAD to STL format conversion of a part, staircase effect due to the layered part construction, machine errors, other process parameters-related errors or those errors associated to material shrinkage during the process, negatively influence the accuracy of manufactured parts. These and other errors have been recognised and analysed in numerous research papers (Bochmann et al., 2015, Umaras and Tsuzuki, 2017) and several strategies have been proposed for their attenuation.

Among the lines of research focusing on geometric distortion compensation, those that address the problem by modifying the nominal geometry of the CAD model stand out (Noriega et al., 2013, Xu et al., 2017, Beltrán et al., 2021, Zhang and Anand, 2020, Navangul et al., 2013). Within this strategy, Noriega et al. (2013) developed a predictive model based on Artificial Neural Networks (ANN) to predict dimensional errors in prismatic parts and compensate for them in the CAD models. Other works parameterise the CAD model to establish a correspondence between it and the surfaces of the manufactured part in order to determine and compensate for geometric deviations. Such is the case of Xu et al. (2017), who use markers distributed along the geometry to establish a correspondence between the manufactured part and the CAD model. Likewise, Beltrán et al. (2021) apply a similar methodology on cylindrical parts, parameterising the geometry based on generatrices and circular sections to compensate for the deviations actually measured with a coordinate measuring machine (CMM) on the part surface. Another example of parameterisation is proposed by Zhang and Anand (2020) who, based on the deviations information obtained by a predictive model, perform the compensation of the CAD model by means of a NURBS-adjusted surface.

Other authors, such as Navangul et al. (2013), propose to modify the STL file to minimise the chordal errors with respect to the original CAD model and thus improve the accuracy of the manufactured part. Similarly, Zha and Anand (2015) apply a methodology to improve the mesh density in the STL model locally to minimise chordal errors in the most complex areas of the geometry. Other authors apply strategies that modify the geometry resulting from the slicing of the STL model prior to fabrication. For example, Senthilkumaran et al. (2008) experimentally characterise shrinkage in a Selective Laser Sintering (SLS) process and compensate for it by altering the length of each laser track within each layer.

There are works where the compensation strategy is based on modifying the AM process parameters. Some of them apply adaptive slicing techniques that locally optimise the distance between the slicing planes applied to the STL model, adapting the layer thicknesses to the part geometry complexity and to the machine control characteristics (Siraskar et al., 2015, Chen et al., 2021). Other studies address the problem by optimising the characteristic process parameters according to the shrinkage measured in different directions (Sond et al., 2009, Raghunath et al., 2007).

On the other hand, it must be taken into account that many of the errors that appear on the part are due to the operating behaviour of the machine (e.g., inertias, vibrations, geometric deviations of axes, control errors, etc.). To this end, several researchers have developed artefacts of different types such as cylindrical (Tong et al., 2008), hole arrays (Majarena et al., 2017) or stepped pyramids (Zapico et al., 2022) that provide data on the geometric error map over the entire working volume of the machine. From this volumetric error map, mathematical models describing the kinematic behaviour as a function of the analysed machine architecture are adjusted and applied to compensate for the expected deviations. Other research focusing on kinematics pay attention to the quality of material deposition (Ren et al., 2021). In this case, the authors compensate for the filling errors in the parts by means of an experimental model that analyses the evolution of the bead width along rectilinear paths.

Another common way to compensate for complex deformations during an AM process is through the use of predictive models based on finite element techniques (FEM). Some of these studies develop strategies to predict the shrinkage that takes place during the curing stage in a Stereolithography process (Hur et al., 1998, Huang et al., 2003, Huang et al.,

2005, Yaghi et al., 2019). Others describe geometric compensation strategies by reversing FEM-simulated deviations on different AM techniques: Powder Bed Fusion (PBF) (Yaghi et al., 2019, Biegler et al., 2020, Frigioescu et al., 2020), Direct Energy Deposition (DED) (Nguyen et al., 2021), Selective Laser Melting (SLM) (Afazov et al., 2017a) or Wire-Arc Additive Manufacturing (WAAM) (Afazov et al., 2017b). In the case of Afazov et al. (2021), they also apply geometric compensations by reversing the deformations detected by digitising with a 3D scanner.

The current rise in the application of machine learning techniques to multiple fields of engineering has led to their extension to geometric error compensation based on data-driven analysis strategies. Some authors approach the problem by producing multiple batches of parts to iteratively determine the optimal compensation to apply (Hatmann et al., 2019). In contrast, Cheng et al. (2018) address the error compensation problem by modelling the *in-plane* shape deviations as a Gaussian process in which variables related to the process parameters are also considered. Shen et al. (2019) apply a neural network-based model to predict and compensate for the expected deformations from the 2D images of the masks used in a Digital Light Processing (DLP) process. Within this same category, Decker et al. (2021) establish a nonparametric model to predict form accuracy of 3D printed products by learning from triangular meshes of a small set of training shapes.

Finally, some works used the concepts of *in-plane* and *out-of-plane* to model and compensate for the geometric deviations that occur respectively in the X-Y and Z directions of AM parts. In various of these works, the geometric compensation of *in-plane* deviations for polygonal (Huang et al., 2014), cylindrical (Huang et al., 2015) or freeform (Luan et al., 2016) parts is proposed. Subsequent work describes an optimised compensation model to minimise deviations in 2D (minimum area deviation) and 3D (minimum volume deviation) (Huang et al., 2016). Among other sources, they also studied the influence of extruder positioning error in a Fused Filament Fabrication (FFF) machine on material deposition (Wang et al., 2016). To optimise the 3D compensation methodology, they conducted a study to determine the interaction that appears between adjacent layers (Jin et al., 2020) and established a convolution-based formulation to model the distortions due to this phenomenon (Huang et al., 2020). Some of the most recent works model deflections using Bayesian Neural Networks (Ferreira et al., 2019) or by models capable of predicting deflections, both in geometries with smooth curvatures and with abrupt changes (Wang et al., 2022).

The aforementioned works describe different methodologies to meet the common goal of compensating for geometric distortions originated during the AM process. Most of them are based on the use of analytical models that require in-depth knowledge of the process or extensive characterisation work. Moreover, many of these models are developed for a specific combination of process or part geometry.

A different approach to address compensation without using this type of models and, therefore, to extend its application to different processes and working conditions, would be the use of methods based on comparing the geometry obtained in the manufacture of the part with respect to its nominal geometry. With this focus, the present paper describes a new methodology for *in-plane* compensation of form and size deviations of each layer deposited when building a part by AM processes. The nominal layer contour extracted from the STL of the part and the actual contour obtained during manufacturing are used as input to this compensation method. The actual contour can be obtained mainly by a digitising process that can be performed either in-situ or off-line. The compensation of the detected deviations is applied to the STL model without modifying the original CAD

model. Two case studies presented in the paper demonstrate the effectiveness of the method. This novel method constitutes an important advance compared to other works, as it is applicable to layers of any shape obtained in any AM process.

2. Layer contour compensation procedure

In an additive manufacturing process, the starting point is a CAD model of a part which, once converted to STL format, is sliced into layers, creating the so-called *nominal contours* (NC) (Figure 1), that will be used to generate the G-code program required to manufacture that part.

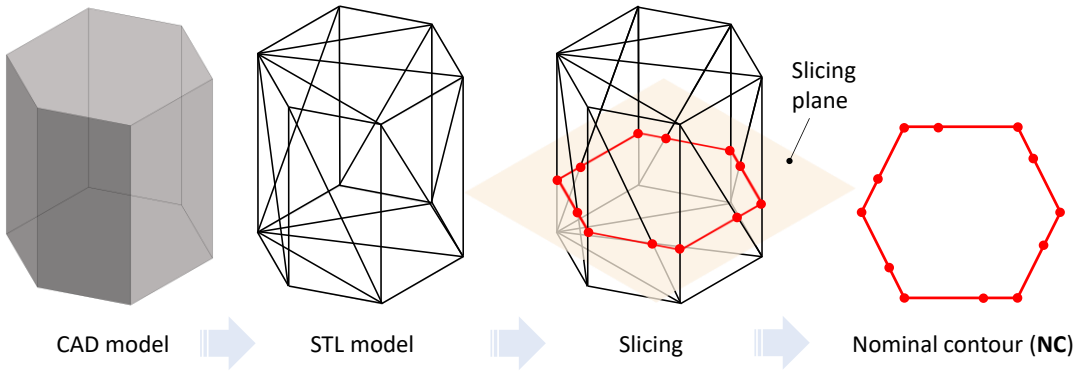

Figure 1. Extraction of a nominal contour (NC) from the CAD model of a part.

Due to different error sources, the actual contour of each manufactured layer deviates from the *nominal contour*. The actual contour will be referred to as the *distorted contour* (DC) hereafter. This contour can be obtained directly, by digitising the manufactured part, or artificially generated by means of a predictive distortion model that simulates the deviations due to both the machine and the process-related errors (Figure 2).

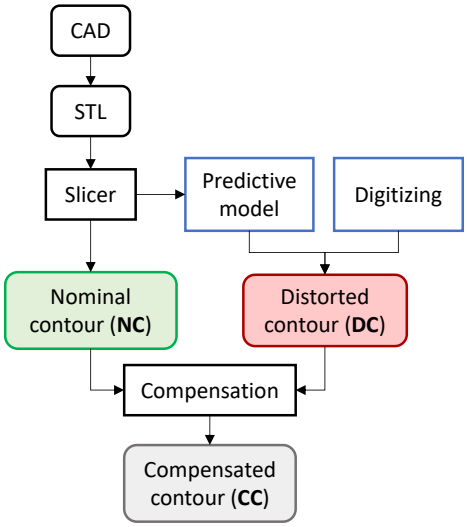

Figure 2. Generation of a *compensated contour* (CC).

The compensation procedure developed here consists in obtaining a *compensated contour* (CC) which, once manufactured, will provide a less distorted real contour. The CC is obtained by comparing the DC versus the NC. This involves four steps: alignment of both contours, determination of form deviations, compensation for these deviations and alignment reversal (Figure 3). Each of these steps are detailed in the following sections.

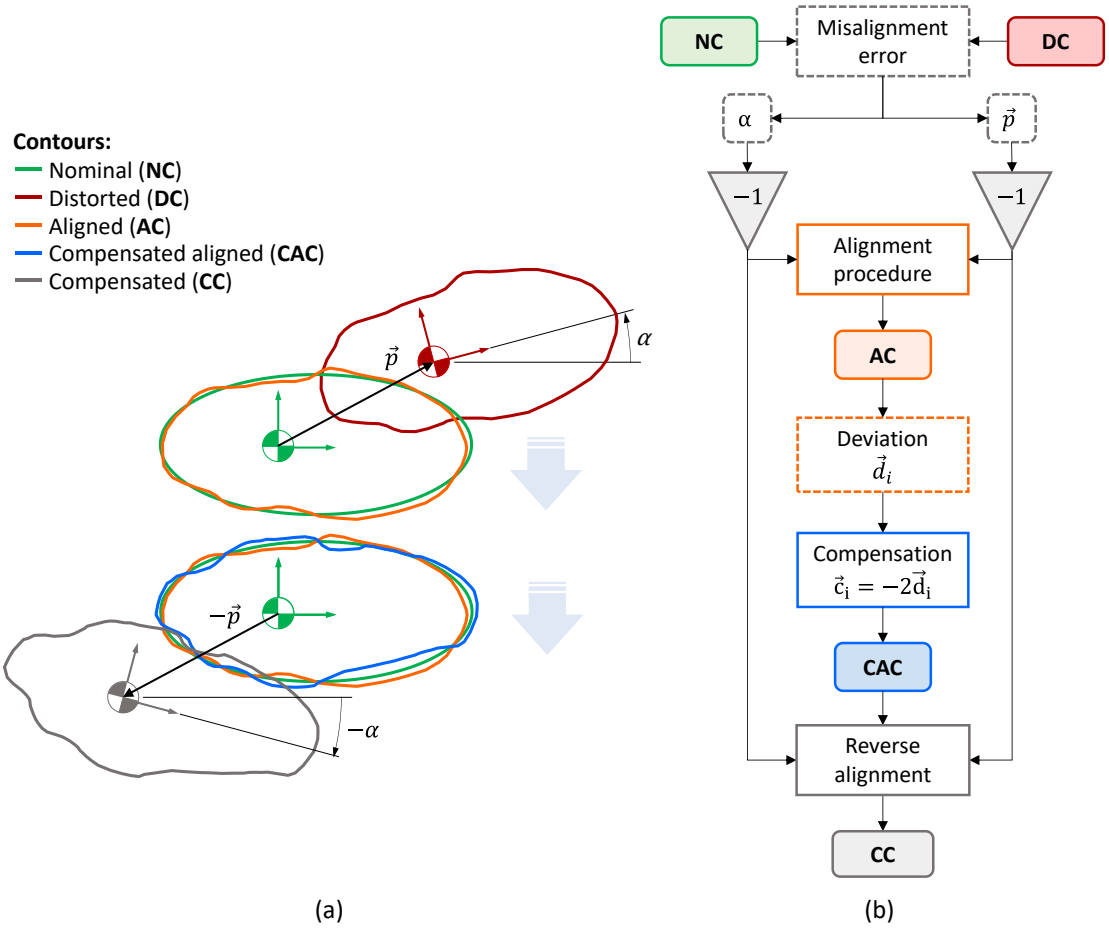

Figure 3. Distorted contour compensation: (a) steps; (b) algorithm.

2.1. Alignment procedure

The alignment procedure consists in a translation $\vec{p}$ and a rotation α of the DC until it matches the NC (Figure 4). The translation $\vec{p}$ represents the 2D-distance between the centroids of both contours (O_1 and O_2), whereas the rotation α is the angular offset between both contours after matching the centroids.

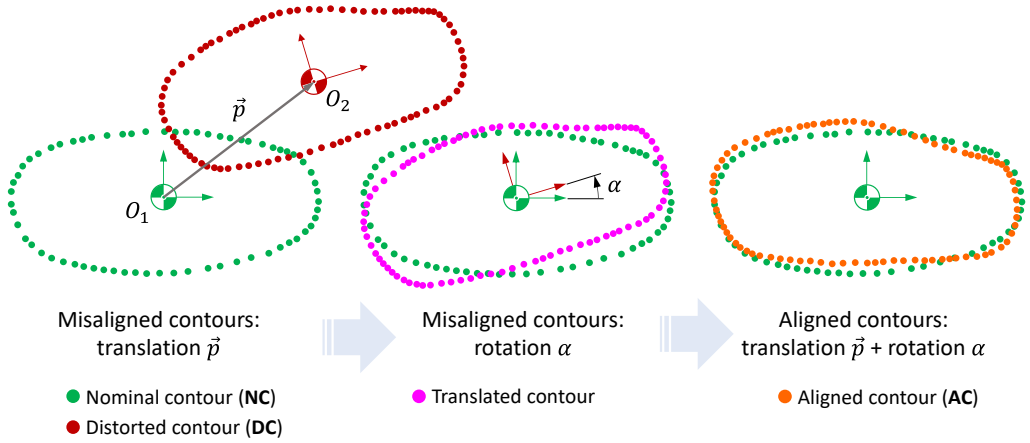

Figure 4. Alignment procedure: translation and rotation.

The steps necessary to align the DC and the NC are as follows:

1. Determine the centroids O_1 and O_2 corresponding to each contour and calculate the

translation vector $\vec{p}$.

2. Perform the translation of the DC points by applying the opposite of vector $\vec{p}$. The resulting contour will be the so-called *translated contour*.
3. Calculate the principal directions for each contour using the *Principal Component Analysis* (PCA) method.
4. Determine rotation α as the angular difference between the principal directions of both contours.
5. Rotate the *translated contour* counteracting α to obtain the so-called *aligned contour* (AC).

This procedure can be applied to different types of geometric contours. Other alternative registration procedures that could be used are the *Iterative Closest Point* (ICP) or the *Singular Value Decomposition* (SVD), among others (Bellekens et al., 2014).

2.2. Form errors

Once alignment has been performed, the form errors will quantify the geometric deviation between the AC and the NC.

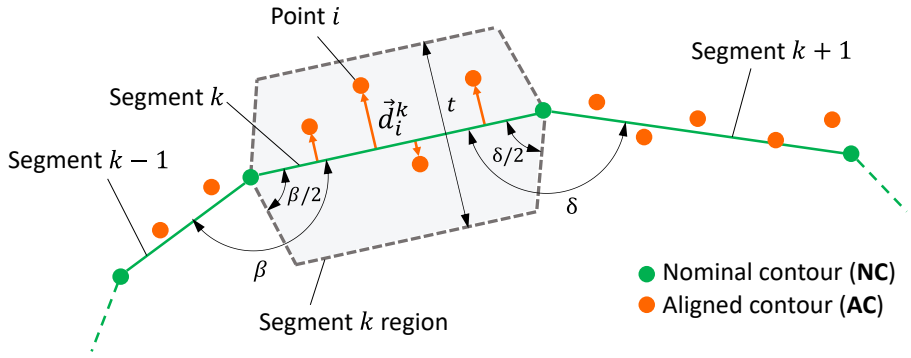

Figure 5. Deviations $\vec{d}_i^k$ of the *aligned contour* points lying within the segment *k* region of the *nominal contour*.

The NC is composed of segments (NC-segments, hereafter) connecting consecutive nominal points. Therefore, the form error calculation algorithm will go along these segments and calculate the minimum 2D-distances between each and the associated points on the AC (AC-points). In this way, for each AC-point i, a deviation vector $\vec{d}_i^k$ will be obtained with respect to the NC-segment k (Figure 5). The AC-points are assigned to a NC-segment if they lie in a region surrounding that segment. Given the feasibility that a point can be assigned simultaneously to two adjacent segments, these regions were defined as shown in Figure 5. The thickness t of the region represents a tolerance value that may be adjusted according to the curvature of the NC, the order of magnitude of deviations to be determined or even the goodness of the alignment process previously performed. Depending on the value of t, some AC-points may lie outside the region and therefore, deviation of these points shall not be considered. An indicator ρ that correlates the number of points within the analysed regions (n_1) and the actual number of AC-points (n_2) is defined as follows:

$$\rho = \frac{n_1}{n_2} \tag{1}$$

Low values of ρ denote a small value of the tolerance t so that it makes necessary to adjust this parameter to a greater value.

2.3. Compensation of form errors

Once obtained the form deviations $\vec{d}_i^k$ between the AC-points and the corresponding NC-segments, the compensation for the calculated errors is carried out by applying a reverse displacement $\vec{c}_i^k = -2\vec{d}_i^k$, obtaining the so-called *compensated aligned contour* (CAC) (Figure 6).

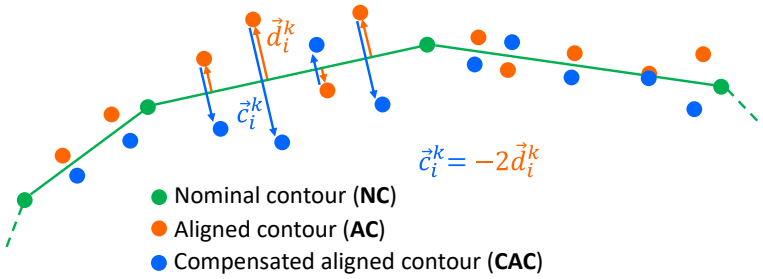

Figure 6. Compensation of form errors.

2.4. Alignment reversal

Once generated the CAC, the alignment with respect to the NC must be undone. For this purpose, reversal translation and rotation operations to those performed at the beginning of the compensation procedure shall be performed (i.e., $-\vec{p}$ and $-\alpha$). This will result in the final *compensated contour* (CC) (Figure 3).

2.5. Quality indicators

In order to evaluate the improvement achieved, some quality indicators were defined to quantify the results before and after applying the compensation algorithm. For this purpose, the following influence factors were taken into account:

- The discrete nature of the compensation algorithm, which considers point deviations that do not fully represent the DC deviations.
- The density of points on the DC (DC-points).
- The number of DC-points lying within the regions obtained from the NC analysed.
- The quality of the alignment between the DC and the NC.

For this reason, a quality indicator so-called *deviation area* (A_c) was defined based on the area contained between the two compared contours (i.e., AC and NC) (Figure 7a). A second indicator considered was the so-called *normalised deviation* (γ) between the AC and the NC, calculated as follows:

$$\gamma = \frac{A_c}{L_p} \tag{2}$$

where L_p is the perimeter of the NC. This indicator reflects the severity of the deviations in relation to the layer size. In this way, it is possible to compare deviations between layers of different size. Therefore, the lower γ, the better matching between the compared contours.

A third indicator considered was the *deviation range* (d_R), which estimates the interval between the maximum (d_{Max}) and minimum (d_{Min}) deviations with respect to the NC where deviations of all the points on the AC lie in (Figure 7b).

$$d_R = d_{Max} - d_{Min} \tag{3}$$

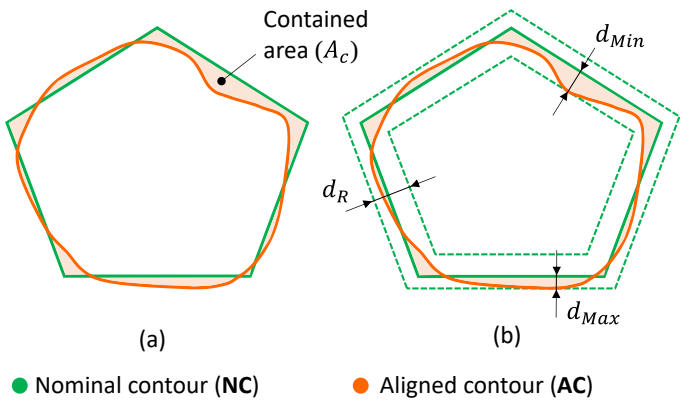

Figure 7. Deviation area, maximum and minimum deviations and deviation range between the AC and the NC.

3. Case study 1

To demonstrate the capabilities of the contour compensation algorithm developed and its applicability to AM, several examples of complex-geometry-profile parts are presented. The profiles considered here were inspired on the well-known Burmester templates or *French Curves*, traditionally used for drawing smooth or conic curves (Figure 8). In this case, the parts were not really manufactured, so the layer contours included geometric distortions obtained artificially, by simulating the AM process with a predictive distortion model that estimates the behaviour of both the material and the machine during manufacturing.

Figure 8. Example parts: Burmester templates.

The slicing process described in section 2 to extract the NCs was carried out by using *CuraEngine*, which starts by processing the geometric information and ends by generating the G-code program. By means of a self-developed routine that interacts with *CuraEngine*, it was possible to export and import a data structure in which the coordinates of the NP-points corresponding to all the layers generated in the slicing process were stored.

In this example, the DCs will be generated artificially by means of a predictive model that simulates the distortions derived from both the machine and the process errors. The study has been particularly applied to parts obtained by FFF. The predictive distortion model is described following.

With regard to the geometric errors in a FFF machine, the model represents the position of the nozzle expressed in the machine reference system by considering the kinematic errors of the different machine axes. This requires knowing these errors (linearity, straightness, squareness) and traverse the kinematic chain by linking the nozzle to the reference system (Tong et al., 2008, Majarena et al., 2017). For simplicity, the proposed model only considered the most influencing errors: the linear errors on the X and Y axes (δ_{xx} and δ_{yy}) and the quadrature error between both axes δ_{xy}. The values considered in

this work (Table 1) were similar to those used by other authors for this type of machines (Bochmann et al., 2015, Majarena et al., 2017, Tong et al., 2003, Cajal et al., 2016).

Table 1. Parameter values considered in the FFF machine error model.

Error	Value
δ_{xx}	5E-3 · x
δ_{yy}	-5E-3 · y
δ_{xy}	1E-2 · y

On the other hand, regarding the process errors, the Yaman's thermal shrinkage model (Yaman, 2018, Diberoglu et al., 2019) was applied, which relates the manufactured part shrinkage to the gradient between glass transition temperature of the deposited material and room temperature. Table 2 shows the parameters used by the model.

Table 2. Parameter values used in the thermal shrinkage model for an FFF process (Cosine, 2021).

Parameter	Value
Material	PLA
T_g [(1)]	60°C
T_R [(2)]	20°C
α [(3)]	6.8 E-5 °C^{-1}

[(1)] Glass transition temperature
[(2)] Room temperature
[(3)] Thermal expansion coefficient

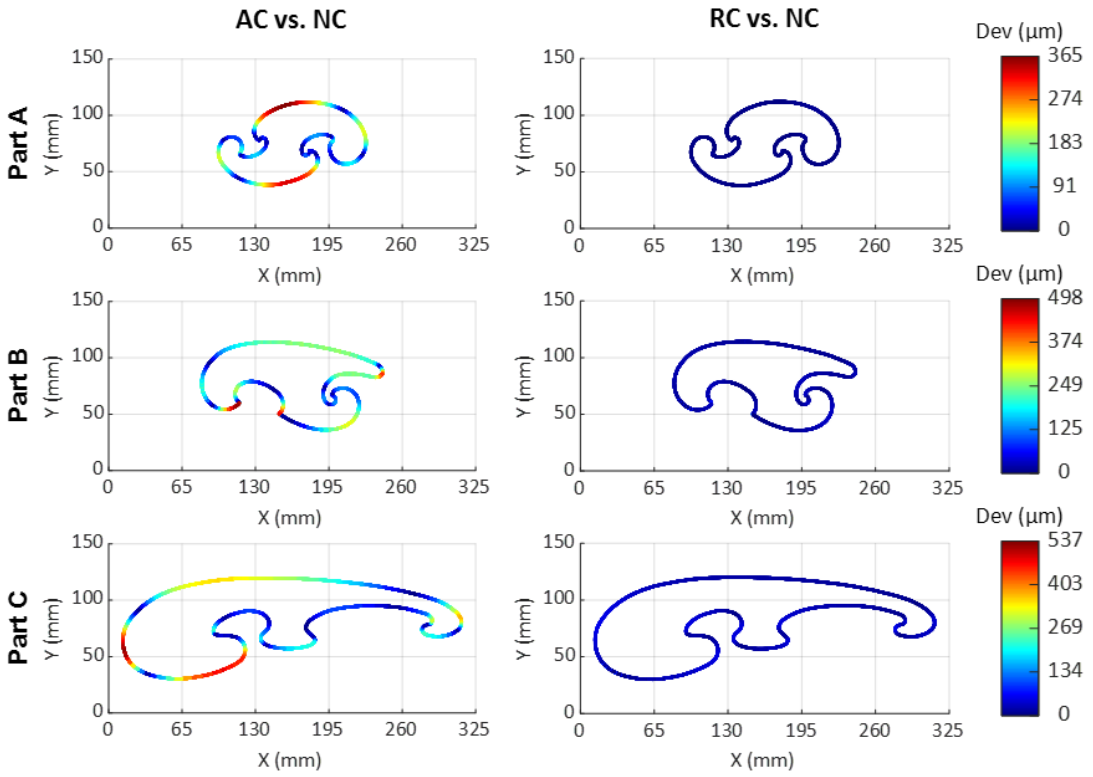

Figure 9. Contour deviations before applying the compensation (AC vs. NC) and deviations of the RCs (RC vs. NC).

The compensation procedure described in section 2 was applied to the DCs to obtain the CCs and create a new STL part model (compensated STL) from them. Presumably, a new part produced from this STL should result in smaller deviations from the nominal geometry. In this case study, the compensated STL was considered as if it were a new part to which the predictive distortion model was applied. The *resulting contours* (RC) should have a similar form to those of the original part, and the better the compensation model developed, the better the match. Thus, to analyse the effectiveness of this model, the deviations of the contours before applying the compensation (AC vs. NC) and those of the resulting contours (RC vs. NC) were compared, as shown in Figure 9. On the other hand, Table 3 shows the quality indicators obtained for these contours.

Table 3. Quality indicators obtained for parts A, B and C.

Part	Compared contours	d_{Min} (mm)	d_{Max} (mm)	d_R (mm)	A_c (mm^2)	γ (µm)
A	*AC vs. NC*	-0.365	0.220	0.585	66.52	147
	RC vs. NC	-0.038	0.040	0.078	0.99	2
B	*AC vs. NC*	-0.498	0.470	0.968	94.78	181
	RC vs. NC	-0.075	0.116	0.191	8.55	16
C	*AC vs. NC*	-0.487	0.538	1.025	161.39	194
	RC vs. NC	-0.071	0.115	0.186	21.55	26

Both Figure 9 and Table 3 show that the RC exhibit a clear improvement compared to the AC geometry, both for the value of deviations and for the different indicators considered. For instance, the normalised deviations γ in the AC vs. NC analysis show deviations of almost 0.2 mm, while this indicator in the RC vs. NC study is at least one order of magnitude lower.

Deviation distributions of the AC vs. NC and RC vs. NC are shown for the three parts as a histogram in Figure 10. In any case, deviations of the RCs show a null deviation central trend, while the ACs present much higher dispersion. The simultaneous interpretation of the histograms and the quality indicators demonstrate the effectiveness of the developed compensation model.

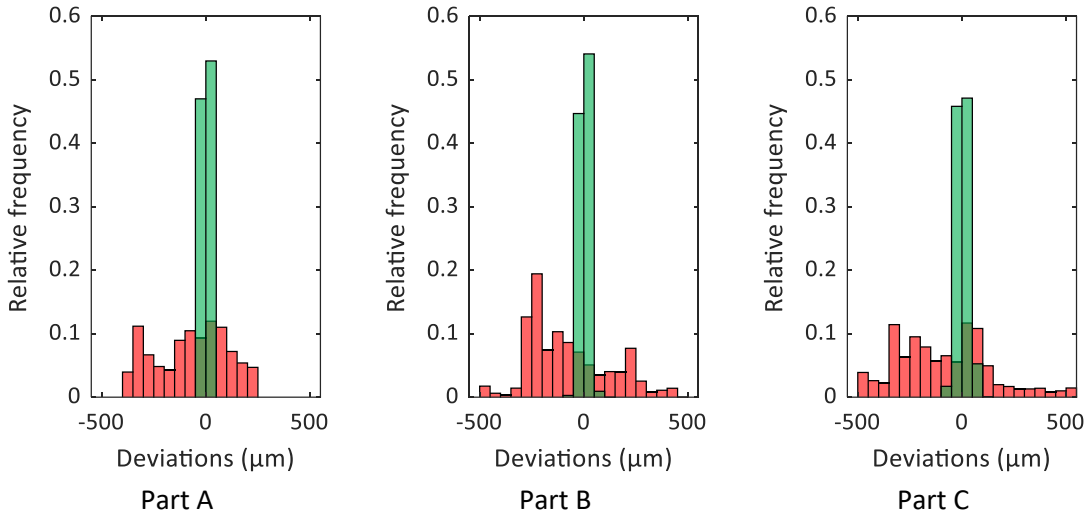

Figure 10. Deviation distributions of AC vs. NC (red) and RC vs. NC (green) of the test part in the case study 1.

4. Case study 2

In this second case study, the contour compensation algorithm developed was applied to a real part manufactured in PLA by means of a FFF AM machine developed by Peña et al. (2021) (Fig 11a). The test part consisted of seven 10 mm high steps, each with a curvilinear contour (Fig 11b). The main processing parameters used are shown in Table 4.

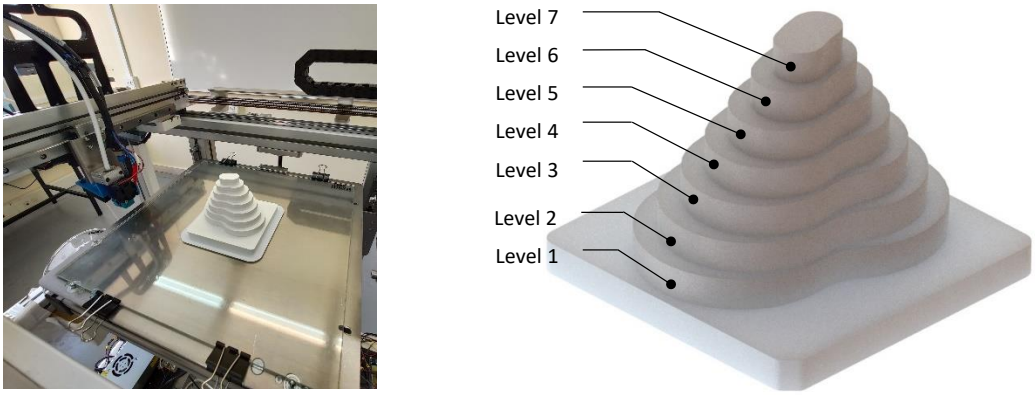

Figure 11. (a) The test part in the FFF machine; (b) test part geometry.

Table 4. Process parameters used in the FFF machine to build the test parts.

Parameter	Value
Layer thickness (mm)	0.1
Infill (%)	20
Nozzle temperature (ºC)	200
Bed temperature (ºC)	58

Once manufactured, the part was measured in a CMM in order to obtain the DCs that represent each step. A DEA Global Image CMM was used for this purpose, equipped with a motorized indexable head Renishaw PH10-MQ, a SP25M continuous scanning probe and a 30 mm long ceramic stylus tip with a 3 mm diameter ruby ball. The maximum repeatability ($R_{0,MPL}$) and the maximum admissible error ($E_{0,MPE}$) according to ISO 16360-2:2010 are the following:

$$R_{0,MPL} = 2.2\ \mu m \tag{4}$$

$$E_{0,MPE} = 2.2 + 3L \cdot 10^{-3}\ \mu m, \text{being } L \text{ in mm} \tag{5}$$

For each step, the measurement procedure consisted in a continuous scanning at three different heights (Figure 12). By applying a 3σ Gaussian filter to the three acquired contours, the resultant average contour was used as the DC. These contours were then processed and converted into the CCs. A compensated STL model was created from these and then used to build a new test part on the FFF machine. The resulting part was measured on the CMM in the same way as the initial test part, so that the RCs were obtained.

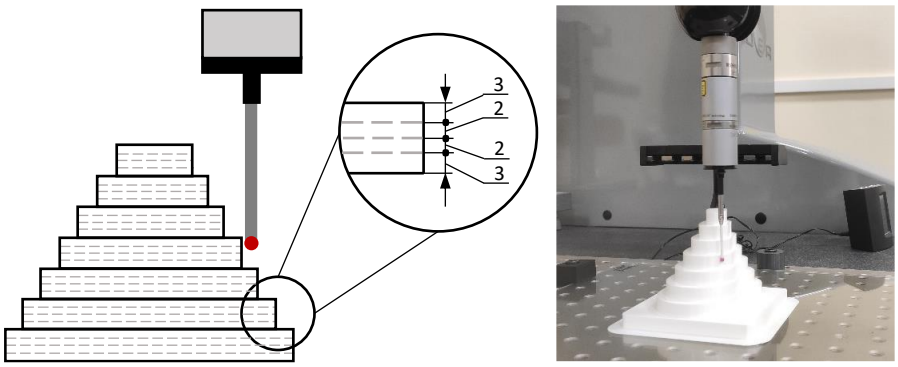

Figure 12. CMM continuous probing at each step of the example part.

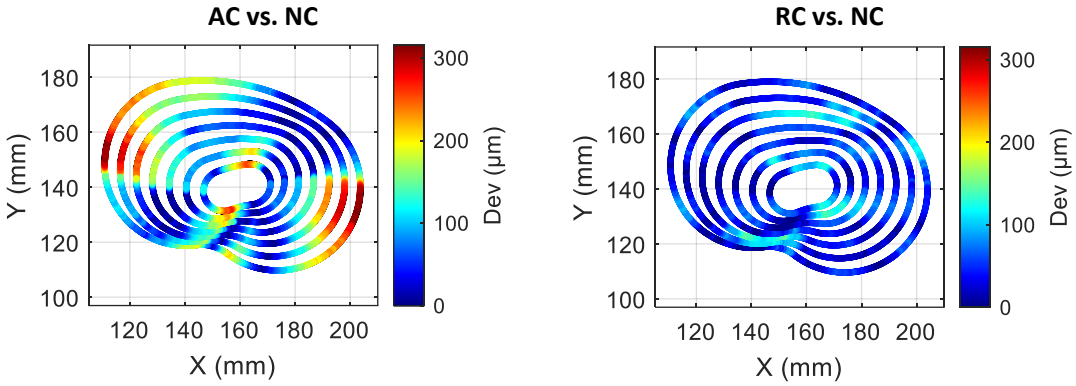

Figure 13. Contour deviations for the test part before (AC vs. NC) and after (RC vs. NC) applying the compensation procedure.

For the study of results, the deviations obtained between the ACs and RCs with respect to the NCs were compared. The ACs were obtained from the DCs measured on the initial test part and the RCs from the final test part. The deviations obtained in each case are represented in Figure 13 and the value of the quality indicators in Table 5.

Table 5. Quality indicators obtained for the test parts.

Step	Compared contours	d_{Min} (mm)	d_{Max} (mm)	d_R (mm)	A_c (mm^2)	γ (µm)
1	*AC vs. NC*	-0.316	0.212	0.528	38.96	150
	RC vs. NC	-0.097	0.124	0.221	11.13	43
2	*AC vs. NC*	-0.294	0.158	0.452	28.89	128
	RC vs. NC	-0.124	0.090	0.214	10.83	48
3	*AC vs. NC*	-0.264	0.111	0.375	18.68	97
	RC vs. NC	-0.153	0.082	0.235	11.90	62
4	*AC vs. NC*	-0.185	0.103	0.288	11.92	74
	RC vs. NC	-0.093	0.097	0.190	6.88	43
5	*AC vs. NC*	-0.205	0.053	0.258	10.53	81
	RC vs. NC	-0.031	0.114	0.145	6.13	47
6	*AC vs. NC*	-0.229	0.055	0.284	8.95	92
	RC vs. NC	-0.021	0.148	0.169	5.57	57
7	*AC vs. NC*	-0.270	0.029	0.299	7.55	113
	RC vs. NC	-0.003	0.131	0.134	4.41	66

As it was expected, Figure 13 shows a clear improvement of deviations detected between the test parts manufactured initially (AC vs. NC) and after applying the compensation (RC vs. NC) procedure. Furthermore, Table 5 also reflects an improvement in all the quality indicators for all the steps. For instance, the indicator for the normalised deviations γ in the AC vs. NC varies within a range of 76 µm whereas this indicator lies within a range of 23 µm in the case of RC vs. NC (Figure 14). This reveals not only a matching improvement between both contours but also a uniformity of deviations in all the steps.

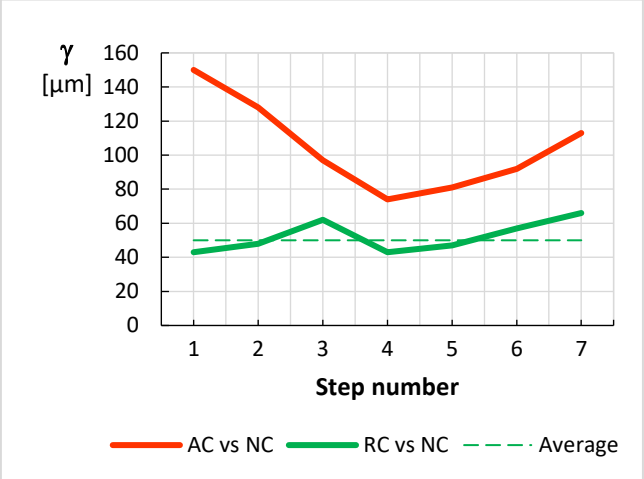

Figure 14. Normalised deviation indicator (γ).

Figure 15 shows the deviation distributions of both the AC vs. NC and RC vs. NC cases. It can be noted the important reduction of the dispersion of deviations as well as the central trend of deviations is close to zero in steps 1 to 4 and slightly higher in steps 5 to 7. There seems to be a tendency for the central value of the distribution to move away from the null deviation as the step size becomes smaller. This could be due to the loss of precision in the contour alignment procedure the smaller the contours are or even due to the influence of the process parameters used to build the test parts. For example, both the wall thickness and the infill were the same regardless of the step considered so different shrinkage could have occurred which would have affected small versus large steps differently. In any case, a clear improvement in the quality of the compensated part is achieved.

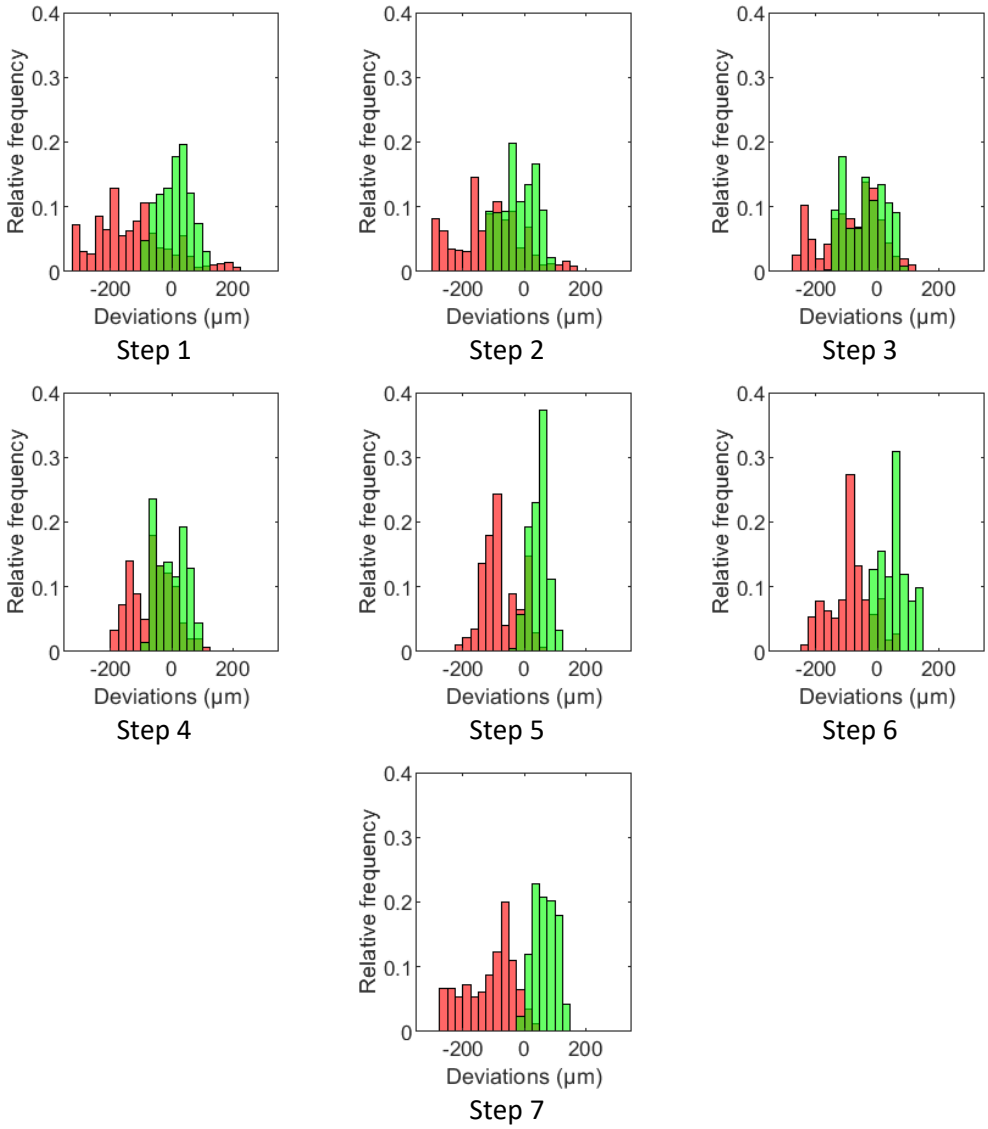

Figure 15. Deviation distributions of AC vs. NC (red) and RC vs. NC (green) of the test part in the case study 2.

5. Conclusions

This work provides a new procedure for *in-plane* compensation of geometric errors that commonly appear in the layers deposited by an AM process when manufacturing a part, regardless of the complexity of the layers geometry or the AM process used. This procedure is based on comparing the actual layer contours with respect to the nominals extracted from the STL model of the part. Taking into account both alignment errors and form deviations, the compensation algorithm generates new compensated contours matching the nominals as much as possible. To evaluate the compensation effectiveness, several quality indicators were considered.

The compensation method was applied to two case studies corresponding to parts with complex geometry. The parts in the first case study were not manufactured but the distortions were simulated by means of a predictive model that considered both the machine and the process errors. In the second example, the test part was actually manufactured and the distortions were measured on a CMM. In both cases, the geometric deviations detected and the quality indicators calculated were significantly improved after applying the compensation procedure. This means that the compensated and nominal

contours match better in both shape and size. However, the results of the second case study reveal dimensional overcompensation when applied to small contours, where average deviations of around 90 µm are observed, while zero average deviations are achieved for large contours.

Although the improvements achieved can be considered sufficient for the process FFF used in the case studies, the compensation procedure could be enhanced if the compensation factor applied took into account the layer contour size under analysis as well as other process parameters. This would require further experimental development, dealing with geometries varying in shape and size.

The application of this method to industrial production requires the sacrifice of the first part, used for the analysis of geometric deviations. Its cost-effectiveness is therefore justified in the production of medium or large series, or even in short series if it is used in processes with high precision requirements.

References

Afazov, S., Denmark, W. A., Toralles, B. L., Holloway, A., & Yaghi, A. (2017a). Distortion prediction and compensation in selective laser melting. Additive Manufacturing, 17, 15–22. https://doi.org/10.1016/j.addma.2017.07.005.

Afazov, S., Okioga, A., Holloway, A., Denmark, W., Triantaphyllou, A., Smith, S. A., & Bradley-Smith, L. (2017b). A methodology for precision additive manufacturing through compensation. Precis. Eng., 50, 269–274. https://doi.org/10.1016/j.precisioneng.2017.05.014.

Afazov, S., Semerdzhieva, E., Scrimieri, D., Serjouei, A., Kairoshev, B., & Derguti, F. (2021). An improved distortion compensation approach for additive manufacturing using optically scanned data. Virtual and Physical Prototyping, 16(1), 1–13. https://doi.org/10.1080/17452759.2021.1881702.

Bellekens, B., Spruyt, V., Berkvens, R., & Weyn, M. (2014). A survey of rigid 3d pointcloud registration algorithms. In AMBIENT 2014: the Fourth International Conference on Ambient Computing, Applications, Services and Technologies, August 24-28, 2014, Rome, Italy (pp. 8–13).

Beltrán, N., Álvarez, B. J., Blanco, D., Peña, F., & Fernández, P. (2021). A Design for Additive Manufacturing Strategy for Dimensional and Geometrical Quality Improvement of PolyJet-Manufactured Glossy Cylindrical Features. Polymers, 13(7), 1132. https://doi.org/10.3390/polym13071132.

Biegler, M., Elsner, B. A., Graf, B., & Rethmeier, M. (2020). Geometric distortion-compensation via transient numerical simulation for directed energy deposition additive manufacturing. Sci. Technol. Weld. Joi., 25(6), 468–475. https://doi.org/10.1080/13621718.2020.1743927.

Bochmann, L., Bayley, C., Helu, M., Transchel, R., Wegener, K., & Dornfeld, D. (2015). Understanding error generation in fused deposition modeling. Surface Topography: Metrology and Properties, 3(1), 014002. https://doi.org/10.1088/2051-672X/3/1/014002.

Cajal, C., Santolaria, J., Samper, D., & Velazquez, J. (2016). Efficient volumetric error compensation technique for additive manufacturing machines. Rapid Prototyping J., 22(1), 2–19. https://doi.org/10.1108/RPJ-05-2014-0061.

Chen, Q., Xu, J., & Zhang, S. (2021). Cylindricity and flatness optimization for

mechanical parts in additive manufacturing based on tolerance adaptive slicing. Int. J. Adv. Manuf. Technol., 115(11), 3839–3857. https://doi.org/10.1007/s00170-021-07271-4.

Cheng, L., Wang, A., & Tsung, F. (2018). A prediction and compensation scheme for in-plane shape deviation of additive manufacturing with information on process parameters. IISE Transactions, 50(5), 394–406. https://doi.org/10.1080/24725854.2017.1402224.

Cosine Additive, Inc. Large scale 3D printing. [online] Available at: https://www.cosineadditive.com/en/materials/#pla [Accessed 15 November 2021]

Decker, N., Lyu, M., Wang, Y., & Huang, Q. (2021). Geometric accuracy prediction and improvement for additive manufacturing using triangular mesh shape data. J. Manuf. Sci. Eng., 143(6), 061006. https://doi.org/10.1115/1.4049089.

Dilberoglu, U. M., Simsek, S., & Yaman, U. (2019). Shrinkage compensation approach proposed for ABS material in FDM process. Materials and Manufacturing Processes, 34(9), 993-998. https://doi.org/10.1080/10426914.2019.1594252.

Ferreira, R. D. S. B., Sabbaghi, A., & Huang, Q. (2019). Automated geometric shape deviation modeling for additive manufacturing systems via Bayesian neural networks. IEEE Trans. Autom. Sci. Eng., 17(2), 584–598. https://doi.org/10.1109/TASE.2019.2936821.

Frigioescu, T., Matache, G., Badea, T., & Ionita, D. (2020, December). Distortion compensation of IN 625 parts manufactured by selective laser melting. In AIP Conference Proceedings (Vol. 2302, No. 1, p. 120005). AIP Publishing LLC. https://doi.org/10.1063/5.0033743.

Gibson, I., Rosen, D., Stucker, B. & Khorasani, M. (2010). Additive manufacturing technologies (Vol. 17). Cham, Switzerland: Springer. https://doi.org/10.1007/978-3-030-56127-7.

Hartmann, C., Lechner, P., Himmel, B., Krieger, Y., Lueth, T. C., & Volk, W. (2019). Compensation for Geometrical Deviations in Additive Manufacturing. Technologies, 7(4), 83. https://doi.org/10.3390/technologies7040083.

Huang, Q. (2016). An analytical foundation for optimal compensation of three-dimensional shape deformation in additive manufacturing. J. Manuf. Sci. Eng., 138(6), 061010. https://doi.org/10.1115/1.4032220.

Huang, Q., Nouri, H., Xu, K., Chen, Y., Sosina, S., & Dasgupta, T. (2014). Statistical predictive modeling and compensation of geometric deviations of three-dimensional printed products. J. Manuf. Sci. Eng., 136(6), 061008. https://doi.org/10.1115/1.4028510.

Huang, Q., Wang, Y., Lyu, M., & Lin, W. (2020). Shape deviation generator—a convolution framework for learning and predicting 3-D printing shape accuracy. IEEE Trans. Autom. Sci. Eng., 17(3), 1486–1500. https://doi.org/10.1109/TASE.2019.2959211.

Huang, Q., Zhang, J., Sabbaghi, A., & Dasgupta, T. (2015). Optimal offline compensation of shape shrinkage for three-dimensional printing processes. IIE transactions, 47(5), 431–441. https://doi.org/10.1080/0740817X.2014.955599.

Huang, Y. M., & Lan, H. Y. (2005). Dynamic reverse compensation to increase the accuracy of the rapid prototyping system. J. Mat. Process. Tech., 167(2-3), 167–176.

https://doi.org/10.1016/j.jmatprotec.2005.06.029.

Huang, Y. M., and Jiang, C. P. (2003). Curl Distortion Analysis During Photopolymerisation of Stereolithography Using Dynamic Finite Element Method. Int. J. Adv. Manuf. Technol., 21(8), 586–595. https://doi.org/10.1007/s00170-002-1317-z.

Hur, S. S., and Youn, J. R. (1998). Prediction of the Deformation in Stereolithography Products Based on Elastic Thermal Shrinkage. Polym.-Plast. Technol. Eng., 37(4), 539–563. https://doi.org/10.1080/03602559808001379.

Jin, Y., Qin, S. J., & Huang, Q. (2020). Modeling inter-layer interactions for out-of-plane shape deviation reduction in additive manufacturing. IISE Transactions, 52(7), 721–731. https://doi.org/10.1080/24725854.2019.1676936.

Luan, H., & Huang, Q. (2016). Prescriptive modeling and compensation of in-plane shape deformation for 3-D printed freeform products. IEEE Trans. Autom. Sci. Eng., 14(1), 73–82. https://doi.org/10.1109/TASE.2016.2608955.

Majarena, A. C., Aguilar, J. J., & Santolaria, J. (2017). Development of an error compensation case study for 3D printers. Procedia Manufacturing, 13, 864–871. https://doi.org/10.1016/j.promfg.2017.09.145.

Navangul, G., Paul, R., & Anand, S. (2013). Error minimization in layered manufacturing parts by stereolithography file modification using a vertex translation algorithm. J. Manuf. Sci. Eng., 135(3), 031006. https://doi.org/10.1115/1.4024035.

Nguyen, L., Buhl, J., Israr, R., & Bambach, M. (2021). Analysis and compensation of shrinkage and distortion in wire-arc additive manufacturing of thin-walled curved hollow sections. Additive Manufacturing, 47, 102365. https://doi.org/10.1016/j.addma.2021.102365.

Noriega, A., Blanco, D., Alvarez, B. J., & Garcia, A. (2013). Dimensional accuracy improvement of FDM square cross-section parts using artificial neural networks and an optimization algorithm. Int. J. Adv. Manuf. Technol., 69(9), 2301–2313. https://doi.org/10.1007/s00170-013-5196-2.

Peña, F., Fernández, C., Valiño, G., Álvarez, B. J., Rico, J. C., & Mateos, S. (2021). Design and construction of a test bench for the manufacture and on-machine non-contact inspection of parts obtained by Fused Filament Fabrication. IOP Conference Series: Materials Science and Engineering, 1193(1), 012090. https://doi.org/10.1088/1757-899X/1193/1/012090.

Raghunath, N., Pulak, M. & Pandey, M. (2007). Improving accuracy through shrinkage modelling by using Taguchi method in selective laser sintering. Int. J. Mach. Tools Manuf., 47(6), 985–995. https://doi.org/10.1016/j.ijmachtools.2006.07.001.

Ren, J., Wei, A. T., Jiang, Z., Wang, H., & Wang, X. (2021). Improved Modeling of Kinematics-Induced Geometric Variations in Extrusion-Based Additive Manufacturing Through Between-Printer Transfer Learning. IEEE Trans. Autom. Sci. Eng., 19(3), 2310–2321. https://doi.org/10.1109/TASE.2021.3063389.

Senthilkumaran, K., Pandey, P. M., & Rao, P. M. (2008, August). Shrinkage compensation along single direction dexel space for improving accuracy in selective laser sintering. In 2008 IEEE International Conference on Automation Science and Engineering (pp. 827–832). IEEE. https://doi.org/10.1109/COASE.2008.4626479.

Shen, Z., Shang, X., Li, Y., Bao, Y., Zhang, X., Dong, X., ... & Wang, F. Y. (2019,

August). PredNet and CompNet: Prediction and High-Precision Compensation of In-Plane Shape Deformation for Additive Manufacturing. In 2019 IEEE 15th International Conference on Automation Science and Engineering (CASE) (pp. 462–467). IEEE. https://doi.org/10.1109/COASE.2019.8842894.

Siraskar, N., Paul, R., & Anand, S. (2015). Adaptive slicing in additive manufacturing process using a modified boundary octree data structure. J. Manuf. Sci. Eng., 137(1), 011007. https://doi.org/10.1115/1.4028579.

Sood, A. K., Ohdar, R. K. & Mahapatra, S. S. (2009). Improving dimensional accuracy of fused deposition modelling processed part using grey Taguchi method. Mater. Des., 30, 4243–4252. https://doi.org/10.1016/j.matdes.2009.04.030.

Tofail, S. A., Koumoulos, E. P., Bandyopadhyay, A., Bose, S., O'Donoghue, L., & Charitidis, C. (2018). Additive manufacturing: scientific and technological challenges, market uptake and opportunities. Mater. Today, 21(1), 22–37. https://doi.org/10.1016/j.mattod.2017.07.001.

Tong, K., Amine Lehtihet, E., & Joshi, S. (2003). Parametric error modeling and software error compensation for rapid prototyping. Rapid Prototyping J., 9(5), 301–313. https://doi.org/10.1108/13552540310502202.

Tong, K., Joshi, S., & Lehtihet, E. A. (2008). Error compensation for fused deposition modeling (FDM) machine by correcting slice files. Rapid Prototyping J., 14(1), 4–14. https://doi.org/10.1108/13552540810841517.

Umaras, E., & Tsuzuki, M. S. (2017). Additive manufacturing–considerations on geometric accuracy and factors of influence. IFAC-PapersOnLine, 50(1), 14940–14945. https://doi.org/10.1016/j.ifacol.2017.08.2545.

Wang, A., Song, S., Huang, Q., & Tsung, F. (2016). In-plane shape-deviation modeling and compensation for fused deposition modeling processes. IEEE Trans. Autom. Sci. Eng., 14(2), 968–976. https://doi.org/10.1109/TASE.2016.2544941.

Wang, Y., Ruiz, C., & Huang, Q. (2022). Learning and Predicting Shape Deviations of Smooth and Non-Smooth 3D Geometries Through Mathematical Decomposition of Additive Manufacturing. IEEE Trans. Autom. Sci. Eng. https://doi.org/10.1109/TASE.2022.3174228.

Xu, K., Kwok, T. H., Zhao, Z., & Chen, Y. (2017). A reverse compensation framework for shape deformation control in additive manufacturing. J. Comput. Inf. Sci. Eng., 17(2). https://doi.org/10.1115/1.4034874.

Yaghi, A., Ayvar-Soberanis, S., Moturu, S., Bilkhu, R., & Afazov, S. (2019). Design against distortion for additive manufacturing. Additive Manufacturing, 27, 224–235. https://doi.org/10.1016/j.addma.2019.03.010.

Yaman, U. (2018). Shrinkage compensation of holes via shrinkage of interior structure in FDM process. Int. J. Adv. Manuf. Technol., 94(5), 2187–2197. https://doi.org/10.1007/s00170-017-1018-2.

Zapico, P., Peña, F., Valiño, G., Rico, J. C., Meana, V., & Mateos, S. (2022). Virtual-point-based geometric error compensation model for additive manufacturing machines. Rapid Prototyping J., (ahead-of-print). https://doi.org/10.1108/RPJ-02-2022-0052.

Zha, W., & Anand, S. (2015). Geometric approaches to input file modification for part quality improvement in additive manufacturing. J. Manuf. Processes, 20(3), 465–477.

https://doi.org/10.1016/j.jmapro.2015.06.021.

Zhang, B., Li, L., & Anand, S. (2020). Distortion prediction and NURBS based geometry compensation for reducing part errors in additive manufacturing. Procedia Manufacturing, 48, 706–717. https://doi.org/10.1016/j.promfg.2020.05.103.

Captions of tables and figures:

Table 1. Parameter values considered in the FFF machine error model.

Table 2. Parameter values used in the thermal shrinkage model for an FFF process (Cosine, 2021).

Table 3. Quality indicators obtained for parts A, B and C.

Table 4. Process parameters used in the FFF machine to build the test parts.

Table 5. Quality indicators obtained for the test parts.

Figure 1. Extraction of a nominal contour (NC) from the CAD model of a part.

Figure 2. Generation of a *compensated contour* (CC).

Figure 3. Distorted contour compensation: (a) steps; (b) algorithm.

Figure 4. Alignment procedure: translation and rotation.

Figure 5. Deviations $\vec{d}_i^k$ of the *aligned contour* points lying within the segment k region of the *nominal contour*.

Figure 6. Compensation of form errors.

Figure 7. Deviation area, maximum and minimum deviations and deviation range between the AC and the NC.

Figure 8. Example parts: Burmester templates.

Figure 9. Contour deviations before applying the compensation (AC vs. NC) and deviations of the RCs (RC vs. NC).

Figure 10. Deviation distributions of AC vs. NC (red) and RC vs. NC (green) of the test part in the case study 1.

Figure 11. (a) The test part in the FFF machine; (b) test part geometry.

Figure 12. CMM continuous probing at each step of the example part.

Figure 13. Contour deviations for the test part before (AC vs. NC) and after (RC vs. NC) applying the compensation procedure.

Figure 14. Normalised deviation indicator (γ).

Figure 15. Deviation distributions of AC vs. NC (red) and RC vs. NC (green) of the test part in the case study 2.